Region-based convolutional neural network for wind turbine wake characterization from scanning lidars

J A Aird[1], E W Quon[2], R J Barthelmie[1] and S C Pryor[3]

[1]Sibley School of Mechanical and Aerospace Engineering, Cornell University, Ithaca, New York 14850, USA
[2]National Renewable Energy Laboratory, Golden, Colorado 80401, USA
[3]Department of Earth and Atmospheric Sciences, Cornell University, Ithaca, New York 14850, USA

E-mail: J A Aird (jaa377@cornell.edu)

Abstract. A convolutional neural network is applied to lidar scan images from three experimental campaigns to identify and characterize wind turbine wakes. Initially developed as a proof-of-concept model and applied to a single data set in complex terrain, the model is now improved and generalized and applied to two other unique lidar data sets, one located near an escarpment and one located offshore. The model, initially developed using lidar scans collected in predominantly westerly flow, exhibits sensitivity to wind flow direction. The model is thus successfully generalized through implementing a standard rotation process to scan images before input into the convolutional neural network to ensure the flow is westerly. The sample size of lidar scans used to train the model is increased, and along with the generalization process, these changes to the model are shown to enhance accuracy and robustness when characterizing dissipating and asymmetric wakes. Applied to the offshore data set in which nearly 20 wind turbine wakes are included per scan, the improved model exhibits a 95% success rate in characterizing wakes and a 74% success rate in characterizing dissipating wake fragments. The improved model is shown to generalize well to the two new data sets, although an increase in wake characterization accuracy is offset by an increase in model sensitivity and false positive wake identifications.

1. Introduction

The downstream propagation of wind turbine wakes throughout wind turbine arrays can affect wind farm operating conditions and performance and alter aerodynamic and structural loading [1–4]. Offshore and on land, measurements indicate that increased turbulence intensity from propagating wakes increases fatigue loading compared to free-flow conditions [5]. Further, measurements collected on land with meteorological (met) masts and a turbine-mounted lidar found that turbines in fully and partially waked conditions experience reduced power output and increased fatigue loading [6]. Wake-induced power losses are particularly important offshore due to the low ambient turbulent kinetic energy. For example, the mean power production reduction at the Horns Rev I offshore wind farm in Denmark is 12.4% (turbine spacing of 7 rotor diameters, D), and at Lillgrund, Sweden (a spacing of 3.3 to 4.3 D) it is 23% [7]. Wake steering may mitigate wake-induced power losses [8, 9], but requires detailed information regarding wake intensity and dynamic wind farm operation. Wind turbine wake

identification and characterization from real-time observational data, such as scanning lidars, is thus pertinent for condition monitoring, wake steering, and dynamic feedback offshore and on land.

Current methods for automated wake detection or characterization exhibit success when applied to lidar arc (scans at a single elevation angle over a range of azimuth angles) and range-height indicator (RHI) scans (single azimuth angle and multiple elevation angles) with one wake; common methods may approximate the location and extent of the wake's centerline through implementing Gaussian fits to line-of-sight velocity deficits or using a velocity deficit and turbulence profile method [10, 11]. However, automated characterization is difficult when considering lidar arc scans with multiple, dissipating, or asymmetric wakes and often requires a priori knowledge of wind turbine rotor dimensions, scan geometry, or performance metrics [12, 13, 14]. Variations in terrain complexity or scanning conditions (i.e., stability, offshore or land-based scanning domains) further complicate the implementation and success of commonly used methods.

Previous work [15] investigated a novel proof-of-concept implementation of a deep (machine) learning convolutional neural network (CNN) to identify and characterize wind turbine wakes from lidar scans. The model, initially developed using 6 months of lidar arc scan data from a wind farm in complex terrain, utilizes a state-of-the-art object detection CNN called Mask R-CNN [16, 17]. The CNN is utilized to detect and mask (return the exact shape of the object within an image in pixels) objects of various sizes within images and has been implemented in a wide variety of use cases, including facial recognition and identifying topographic features and buildings from remote sensing images [18, 19]. In [15], the proof-of-concept CNN successfully identified and returned the exact shape of dissipating, asymmetric, and multiple wakes simultaneously. Further, the model exhibited high success rates for wake characterization over multiple scan geometries and stability conditions. However, the model was tested and trained on only one data set in the previous work.

The model is now improved and tested for generalizability through application to two novel, independent data sets, in which scanning conditions are markedly different from those in the original scan data set. One data set, collected near a coastal escarpment during the Cornell Prince Edward Island Wind Energy Experiment (PEIWEE), captures wakes from a row of wind turbines [20, 21]. The second data set is collected offshore and features up to four rows of multiple wind turbines in a given scan. The original data set utilized to test and develop the CNN and the PEIWEE data set features stacked lidar plan-position indicator (PPI) scans with most scanning sectors spanning 90° in the azimuth or less, whereas the offshore data set contains full PPI scans encompassing nearly 360° in the azimuth. Improvements to the model in [15] are discussed and the generalization process and results are presented along with examples of model output for each scanning campaign.

2. Methodology

2.1. Experimental campaigns

Three scan campaigns are examined herein: the first, initially used in [15] to train and test the proof-of-concept model, a second data set captured near an escarpment in the Cornell PEIWEE experiment, and a third data set captured from an offshore wind farm in the Baltic Sea (figure 1). Scan campaign parameters and usage methodologies are discussed below.

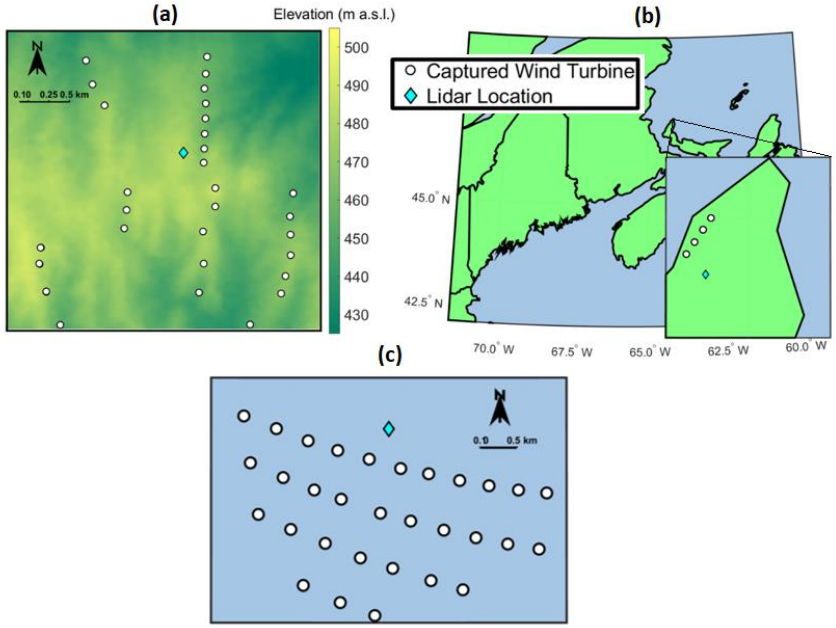

Figure 1. Scanning domain maps for (a) Pacific Northwest (PNW), (b) PEIWEE, and (c) Baltic offshore scanning campaigns. Land is represented by green and sea is represented by light blue. Locations of wind turbines with wakes captured in the scanning campaign are represented by white markers. Location of each scanning lidar is represented by the cyan diamond.

Data set for initial model development (Pacific Northwest [PNW] data set): For the initial proof-of-concept model as described in [15], Mask R-CNN was trained and tested on approximately 270 lidar arc scan images from a scanning campaign of a wind farm in complex terrain. The wind farm is located in the Pacific Northwest of the United States; thus, the data set from this campaign is referred to as the PNW data set. The scans were captured using a WINDCUBE 100 s Doppler wind lidar from Leosphere (described in further detail in [22]). The scans encompass a wide variety of scan parameters, maximum scanning distances, azimuth (α) and elevation (ϵ) angles (predominantly 0° to 4°), and all scans had a range gate resolution of 50 m. Further, the scans were varied rapidly and captured at all times of day, introducing variations in stability and wake characteristics. The data set consisted of approximately four turbines per scan on average, and some scans featured wakes from two rows of turbines to the southwest of the lidar. Cumulative distribution functions of scan parameters for this data set are presented in [15].

Data set for testing model generalizability (PEIWEE data set): The second data set is used to further generalize and improve the model and was collected during the Prince Edward Island Wind Energy Experiment [20]. Arc scan stacks were performed with a Galion pulsed scanning lidar over a period of 2 weeks at the Wind Energy Institute of Canada site on the North Cape of Prince Edward Island. The range gate resolution was 30 m, and each arc scan stack was collected over a 10-minute period. A subset of scan stacks (15 scans) collected over approximately 2 hours in May is considered, in which northerly wake flow from four turbines is visible for all stack elevation angles (2° to 10° in increments of 2°). The terrain is less complex than in the PNW data set, but the flow was over water before encountering the 10–14 m escarpment on which the wind turbines are deployed which impacts mean wind speed and turbulence intensity downwind [20]. A row of four turbines and their corresponding wakes are visible in the scan stacks. The PEIWEE data set is used as an experimental control to evaluate the CNN's generalizability to other data sets.

Data set for testing model generalizability (Baltic data set): The third data set was collected with a Leosphere 200 s scanning lidar at a wind farm offshore in the Baltic Sea and is used to test the improved model's generalizability to offshore scans. In contrast to the other two data sets, scans included in this data set are full PPI scans with azimuthal angles per scan ranging from 1° to 358°. The scans are incremented over a set of elevation angles: 0.5°, 0.7°, 0.9°, 1.4°, and 2.7°. Similar to the PNW data set, the range gate was kept constant across all scans at 50 m. A full scan is collected over a 6-minute period. The wind turbines in the farm are arranged in five rows, and each scan captures approximately five turbines over four rows. Thus, more than 20 wind turbine wakes are visible simultaneously in each of these scans. A subset of approximately 50 scans (collected over a week in April) with subjectively identifiable wakes are considered.

2.2. CNN methodology overview

The CNN applied herein, Mask R-CNN, is a machine learning tool used for a variety of image processing applications. Mask R-CNN takes images as input and performs object detection and instance segmentation, i.e., identifying one or more objects of different types and outlining the shape of those objects within the image; each instance is referred to as a mask.

For this work, lidar scan images containing wind turbine wakes are input into the Mask R-CNN and binary pixel masks indicating wake locations in the images are output. The scan images are cropped at the highest/lowest x and y pixel values, which are recorded and used to convert returned pixel masks to masks measured in meters relative to the lidar. After converting the returned pixel masks to meters, it is then possible to calculate wake characteristics (e.g., the exact shape of the wake, centerline, and wake orientation). The following section describes the CNN methodology in more detail, but we refer to [15] for a thorough description.

Improvements to CNN

The following criteria were imposed in [15] to decide whether a given scan in the PNW data set was included in the data set for model training and testing: wakes had to be unique (could not mix with other wakes in the scan) and discernible (have subjectively identifiable boundaries that may span gaps in the sensing data). For the generalized and improved model discussed herein (Sections 3.1 and 3.2), mixed wake flow cases (cases in which wakes mixed with each other and were subjectively discernible) from the PNW data set were included in model training, increasing the data set count to approximately 300 scans. All previous training parameters used in [15] were kept consistent.

Training the CNN

Scan images are formatted strategically before input into the CNN for testing or training (figure 2). First, the horizontal velocity flow field (figure 2b) is reconstructed from the radial (line-of-sight) velocity flow field (figure 2a) using least-squares linear regression (described in further detail in [15]). This technique, widely used to reconstruct the horizontal flow field, assumes that the flow field is approximately homogeneous and the projection of the vertical wind speed is zero [23, 24]. Next, the flow field is normalized relative to the calculated bulk wind speed per scan (calculated in the process of reconstructing the flow field from least-squares linear regression) to enhance visibility of wakes and low-velocity structures within the flow field image (figure 2c). The final scan format (figure 2d) includes velocity values removed when filtering by carrier-to-noise ratio (CNR), represented in black.

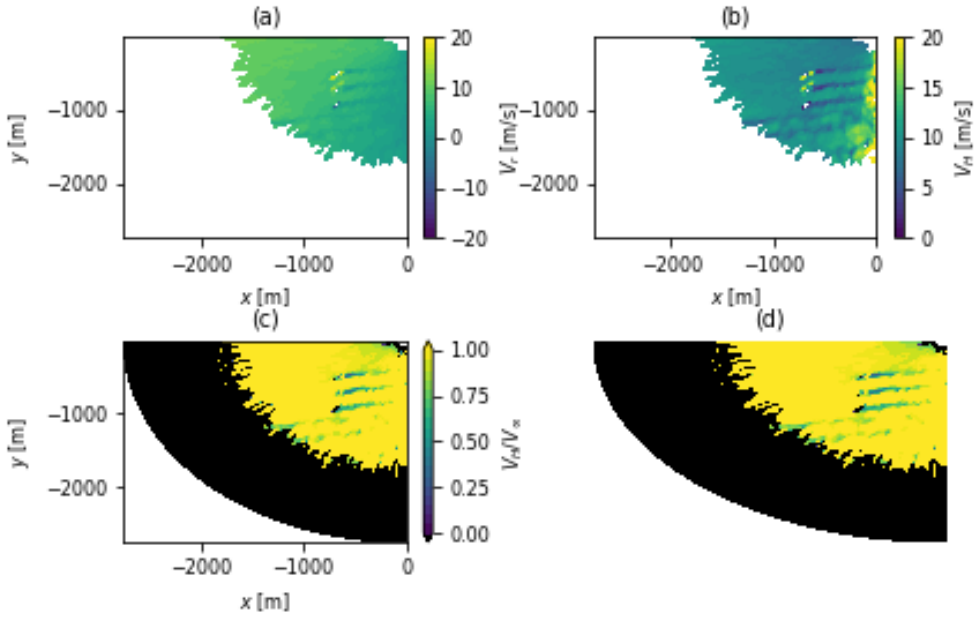

Figure 2. Series of panels depicting velocity field reconstruction from (a,b) radial velocity scan data and (c) flow field normalization for the (d) final scan image for input to the CNN. Lidar scan from PNW data set collected on 02/09/2018 (DD/MM/YYYY) at 04:50 UTC, $\alpha \epsilon [180° - 270°], \varepsilon = 2°$. Dissipating (wake fragments) and obscured (wakes that lie within regions with removed velocity values due to CNR filtering) wakes are visible. Black represents velocity values removed based on the CNR filtering criteria.

3. Results

3.1. Generalization and model improvement results

The proof-of-concept model in [15] exhibits high success rates (see footnote for table 1) for wake characterization (identifying wakes and returning correct masks) when applied to the testing scans from the PNW data set, but low success rates when applied to the PEIWEE data set (table 1, row 2). These contrasting success rates indicate a lack of generalizability within the initial model (note: The PEIWEE data set exhibits no dissipating wake fragments).

To better understand the low success rates, a series of experiments are conducted and results are displayed in table 1. Potential reasons for lack of generalizability include different range gate resolutions (range gates for PNW and PEIWEE data sets are 50 m and 30 m, respectively) and different wake flow directions (westerly for PNW and north-westerly for the PEIWEE data set). Down-sampling the PEIWEE range gate resolution to half of the original resolution results in a reduction in CNN performance (table 1, row 3), indicating the lack of generalizability is not due to differing range gate resolutions between data sets. However, rotating PEIWEE scan images counterclockwise by 90° such that the wakes advect in the same direction as in the training data set results in dramatic increases in model performance (figure 3 and table 1, row 4). This is consistent with expectations, since the R-CNN approach learns “patterns” and thus is inherently sensitive to differences in flow directions between the PEIWEE and PNW data sets.

Increasing the amount of training data by adding more complex wake flow cases from the PNW data set results in markedly improved model accuracy in the initial PNW data set and for all PEIWEE scan configurations considered (down-sampled, rotated). However, both models exhibit improved accuracy when applied to the PEIWEE and Baltic data sets when each is rotated according to the calculated bulk wind direction per scan, β, to depict purely westerly flow (figures 4–6). These findings indicate that the improved CNN model is more robust in characterizing wakes in different flow directions than the initial

model. However, the improved CNN exhibits increased sensitivity to low-velocity flow structures in the field, particularly in regions where the flow is orthogonal to the scanning direction (figure 6) [21]. For the PEIWEE data set, success rates fall when the scans are rotated by β for both models due to enhanced sensitivity to low-velocity flow structures (i.e., more false positives, more of which are counted in the improved CNN model). While there was an increase in the number of true positives (a wake or wake fragment is successfully identified and masked) relative to the data set rotated by 90°, the overall success rate is reduced by false positives (a low-velocity flow structure is incorrectly identified as a wake/wake fragment). Subjectively, these false positives may arise from wake-like structures throughout the scans that could not be attributed to wind turbines and may be attributed to objects (birds, trees) within the flow field. These findings indicate that the models are sensitive to non-wake or wake-like low-velocity flow structures in the scans, but they do successfully identify wakes accurately when they are present. This is further verified in results from the Baltic data set; the improved model exhibits increased accuracy in identifying wakes compared to the proof-of-concept model but slightly less accuracy in identifying wake fragments due to a slight increase in false positives (table 1, row 6). Post-processing steps could thus include limiting CNN output to regions where wakes are expected to occur.

Thus, the conclusions from applying the improved and generalized model are as follows: the improved model more frequently identifies non-wake low velocity structures as wakes than the previous model, particularly in regions where the wind direction is orthogonal to the scanning direction. However, the improved model exhibits improved generalizability to other datasets and an increased rate of true positive wake identification. Thus, the inclusion of the mixed wake cases to the training dataset (as described in 2.2) results in an overall improvement to the model, particularly since post-processing techniques (as mentioned in the previous paragraph) may be applied to further improve results.

Table 1. CNN Wake Characterization Success Rates for Proof-of-Concept [15] and Current CNN Model.

Success Rates[a] – Wake / Wake Fragment Characterization	Proof-of-Concept CNN [15]	Current CNN
PNW Data Set	95%/74%	97%/89%
PEIWEE Data Set	19.1%	39.5%
PEIWEE Data Set (1/2 Range Gate Resolution)	17.1%	36.6%
PEIWEE Data Set (Rotated 90° Counterclockwise)	50.0%	90.0%
PEIWEE Data Set (Rotated by β)	70.1%	67.1%
Baltic Data Set (Rotated by β)	91%/78%	95%/74%

[a] Success rate is calculated over all scans in the testing data sets as success/(fail+success). Sample sizes for PEIWEE, PNW, and Baltic data sets are 15, 59, and 59 scans including approximately 50, 300, and 1180 wakes, respectively. A wake identification is counted as a success when the CNN correctly identifies a wake in the scan and the return mask overlaps with >60% of the subjectively identified wake.

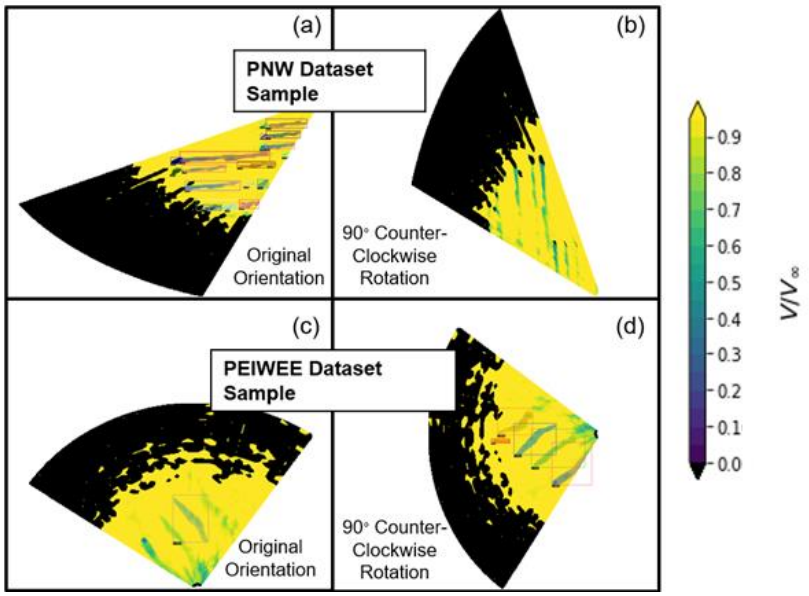

Figure 3. (a, b) Sample scan from the PNW data set used for developing the model shown as wind speed normalized by bulk wind speed per scan estimated through linear regression. Lidar scan collected on 03/11/2018 at 04:59 UTC, $\alpha \epsilon [200° - 240°], \varepsilon = 0.75°$. Wake masks as output by the CNN are shown in color (note: lack of masks in (b) indicates that the CNN did not identify any wakes in the image). (c, d) Sample scan from the PEIWEE data set used for generalizing the model. Lidar scan collected on 13/05/2015 at 15:00 UTC, $\alpha \epsilon [304.5° - 34.5°], \varepsilon = 8°$. Rotations exhibit the improved model's sensitivity to wake flow direction. Black values represent data points removed from the scans during CNR filtering.

3.2. Wake identification and characterization

Regardless of the increase in false positives in some cases, the improved model is preferred over the proof-of-concept model due to its enhanced generalizability. Due to the prevalence of westerly flow in the original model, pre-processing steps when using the CNN will involve rotating the scans by the calculated bulk wind direction, β. As values for β have a degree of uncertainty, particularly in complex terrain, using the model with more robust performance for flow directions near β (i.e., as seen in the counterclockwise 90° rotation success rates) is ideal.

The following figures (figures 4, 5, and 6) depict examples of scan results with the current model. All scan images are rotated by β before input into the current CNN. The goals of the proof-of-concept CNN (simultaneously characterize dissipating, asymmetric, and obscured wakes) are maintained as shown below, and generalizability is improved.

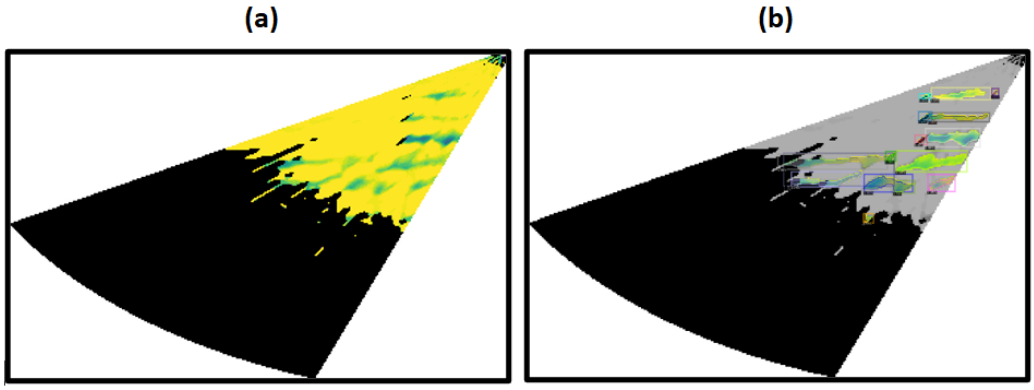

Figure 4. (a) Lidar scan collected on 27/10/2018 at 02:16 UTC, $\alpha \in [200° - 240°], \varepsilon = 0.75°$. (b) CNN output in characterizing (returning pixel masks for wakes within the image) wakes within a PNW scan rotated by β. Dissipating, asymmetric, and obscured (by velocity removal from CNR filtering) wakes are successfully characterized. Wake masks as output by the CNN are shown in color.

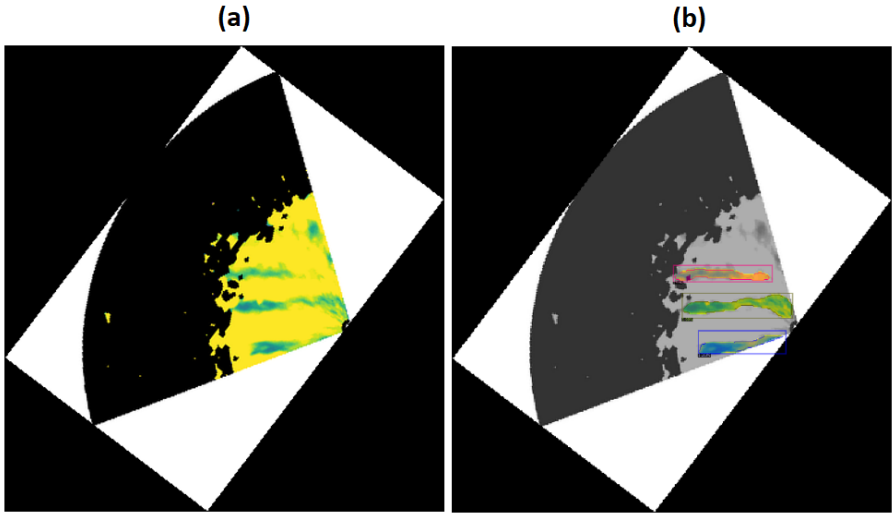

Figure 5. (a) Lidar scan collected on 13/05/2015 at 16:20 UTC, $\alpha \in [304.5° - 34.5], \varepsilon = 8°$. (b) CNN output in characterizing wakes within a PEIWEE scan rotated by β. Asymmetric and obscured wakes are successfully characterized. Wake masks as output by the CNN are shown in color.

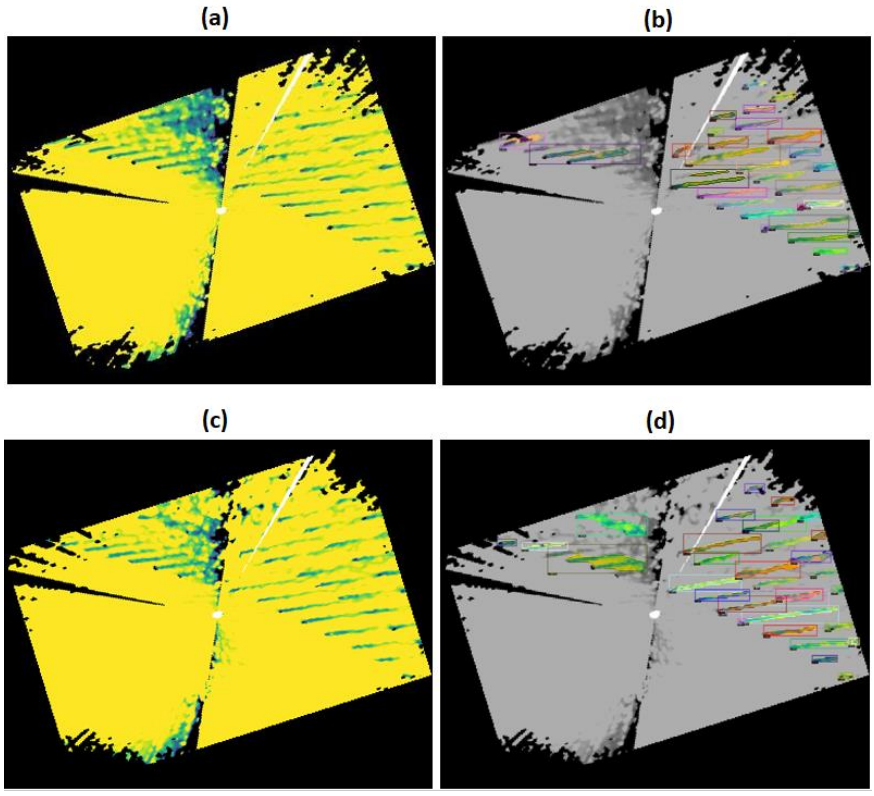

Figure 6. (a) Lidar scan collected on 22/04/2014 at 01:16 UTC, $\alpha \epsilon [1° - 358], \varepsilon = 0.5°$. (b) CNN output in characterizing wakes within a Baltic scan with relatively successful characterization in the region of the flow field affected by wind-lidar directional orthogonality. Obscured and asymmetric wakes are successfully characterized. (c) Lidar scan collected on 22/04/2014 at 01:22 UTC, $\alpha \epsilon [1° - 358], \varepsilon = 0.7°$. Both scan images are rotated by β before input to the CNN.

4. Conclusions

The CNN model from [15] has been improved and generalized through application to two new data sets. The original goals of the proof-of-concept model (further discussed in [15]) included characterization of multiple, dissipating, asymmetric, and obscured wakes (wakes located within regions of removed velocity values due to quality control CNR filtering). The proof-of-concept model was shown to meet these goals. Now, the proof-of-concept CNN, originally trained on a data set of approximately 259 scans in complex terrain, is improved through the addition of approximately 30 new lidar scans to the training subset. Previously, the proof-of-concept model was trained on scans in which wind turbine wakes were unique and subjectively discernible, and wakes could not mix with each other in the event of multiple wakes being present. Now, approximately 30 scans that exhibit wake mixing are included in the training data set, and the improved model exhibits enhanced generalization and wake characterization success rates. The model is further generalized through applying a pre-processing rotation to all scan images such that the wake flow direction is along the same axis.

After model improvement and implementing pre-processing rotation, the model exhibits high accuracy in wake characterization when applied to new lidar scans from an offshore data set in the Baltic Sea. The model was not trained on any scans from this data set. A 95%/74% success rate is calculated for wake/wake fragment (wakes that break and dissipate throughout the flow field) characterization. In contrast, the proof-of-concept model exhibits a 91%/78% success rate for wake/wake fragment

characterization for the same data set. These differences are explained by an increase in model sensitivity exhibited by the improved model; the improved model is more likely to identify low-velocity flow structures in the flow field as wake fragments, but more accurately identifies wakes and wake fragments when they are present. Results further indicate that the improved model is more adept at wake characterization when scans are not oriented such that the flow direction is purely westerly. Post-processing steps may alleviate some of the improved model's increased false positivity rates, such as limiting returned CNN output to regions where wind turbine wakes are expected. This would further improve model output in the event of unexpected objects (birds, trees) within the flow field.

Real-time wake characterization and identification from scanning lidars is pertinent for wake steering applications, potential reduction of fatigue loading, and improving results from scientific wake studies. The model is promising for real-time implementation and scan campaign post-processing due to its demonstrated success when applied to campaigns in offshore/land conditions and to scans that include wakes from more than 20 wind turbines. Further work includes implementing post-processing steps to CNN output to limit returned wakes to regions where wind turbines are expected, and continuing application of the CNN to lidar scans from different campaigns.

Acknowledgements and Funding: The authors are grateful for funding from the National Science Foundation Graduate Research Fellowship Program (DGE-1650441). Funding from the U.S. Department of Energy Office of Energy Efficiency and Renewable Energy and New York State Energy Research and Development Authority via the National Offshore Wind Research and Development consortium (147505) is acknowledged, along with funding from U.S. Department of Energy for the PEIWEE field experiment, project award #: DE-EE0005379. JAA is grateful for her two summer internships at NREL that resulted in this work and is grateful to Paula Doubrawa and Mithu Debnath who helped develop the proof-of-concept CNN model. The authors thank Malik Hassanaly and John Yarbrough for helpful discussions about neural network training. The authors also thank Mithu Debnath for the initial lidar scans that were used in model development and testing and are grateful to Nicholas Hamilton for providing processed scan data for the offshore data set. The authors are grateful for the facilities and personnel at the Wind Energy Institute of Canada (WEICan).

This work was authored in part by the National Renewable Energy Laboratory, operated by Alliance for Sustainable Energy, LLC, for the U.S. Department of Energy (DOE) under Contract No. DE-AC36-08GO28308. Funding provided by the U.S. Department of Energy Office of Energy Efficiency and Renewable Energy Wind Energy Technologies Office. The views expressed in the article do not necessarily represent the views of the DOE or the U.S. Government. The U.S. Government retains and the publisher, by accepting the article for publication, acknowledges that the U.S. Government retains a nonexclusive, paid-up, irrevocable, worldwide license to publish or reproduce the published form of this work, or allow others to do so, for U.S. Government purposes.

References

[1] Eggers Jr A J, Digumarthi R and Chaney K. 2003 *J. Sol. Energy Eng.* **125** 402-409
[2] Hand M M, Kelley N D and Balas M J 2003 *Fluids Engineering Division Summer Meeting* **36967** p. 2557
[3] Barthelmie R J, Hansen K, Frandsen S T, Rathmann O, Schepers J G, Schlez W, Phillips J, Rados K, Zervos A, Politis E S and Chaviaropoulos P K 2009 *Wind Energy* **12** 431-444.
[4] Lee S, Churchfield M, Moriarty P, Jonkman J and Michalakes J 2012 *Proc. of the 50th AIAA Aerospace Sciences Meeting Including the New Horizons Forum and Aerospace Exposition* 9-12 January 2012 Nashville, TN, USA p. 540
[5] Thomsen K and Sørensen P 1999 *J. Wind Eng. Ind. Aerodyn.* **80** 121-136.
[6] Herges T G, Berg J C, Bryant J T, White J R, Paquette, J A and Naughton B T 2018 *J. Phys. Conf. Ser.* **1037** p. 072009
[7] Pryor S C, Barthelmie R J and Shepherd T J 2021 *Joule* **5** 2663-2886
[8] Fleming P, King J, Simley E, Roadman J, Scholbrock A, Murphy P, Lundquist J K, Moriarty P, Fleming K, van Dam J and Bay C 2020 *Wind Energy Sci.* **5** 945-958
[9] Fleming P, Annoni J, Shah, J J, Wang L, Ananthan S, Zhang Z, Hutchings K, Wang P, Chen W and Chen L 2017 *Wind Energy Sci.* **2** 229-239
[10] Quon E W, Doubrawa P and Debnath M 2020 *J. Phys. Conf. Ser.* **1452** p. 012070

[11] Panossian N, Herges T G and Maniaci D C 2018 *2018 Wind Energy Symposium* 8-12 January 2018 Kissimmee, FL, USA p. 0514
[12] Barthelmie R J and Pryor S C 2019 *Atmos. Meas. Tech.* **12** 3463-3484
[13] Aitken M L, Banta R M, Pichugina Y L and Lundquist J K *J. Atmos. Ocean Technol.* **31** 765-787
[14] Herges T G, Maniaci D C, Naughton B T, Mikkelsen T and Sjöholm M 2017 *J. Phys. Conf. Ser.* **854** p. 012021
[15] Aird J A, Quon E W, Barthelmie R J, Debnath M, Doubrawa P and Pryor S C 2021 *Remote Sens.* **13** 4438
[16] Girshick R, Donahue J, Darrell T and Malik J 2015 *IEEE Trans. Pattern Anal. Mach. Intell.* **38** 142-158
[17] He K, Gkioxari G, Dollár P and Girshick R 2017 *Proc. of the IEEE Int. Conf. on Computer Vision* 22-29 October 2017 Venice, Italy p. 2961-2969
[18] Li Y, Xu W, Chen H, Jiang J and Li X 2021 *Remote Sens.* **13** 1070
[19] Maxwell A E, Pourmohammadi P and Poyner J D 2020 *Remote Sens.* **12** 547
[20] Barthelmie R J, Wang H, Doubrawa P, Giroux G and Pryor S C 2016 *Wind Energy* **19** 2271-2286
[21] Wang H, Barthelmie R J, Doubrawa P and Pryor SC 2016 *Atmos. Meas. Tech.* **9** 4123-4139
[22] Thobois L, Krishnamurthy R, Boquet M, Cariou J and Santiago A 2015 *Proc. of the 14th Int. Conf. on Wind Engineering* 21-26 June 2015 Porto Alegre, Brazil
[23] Smalikho I 2003 *J. Atmos. Ocean. Technol.* **20** 276-291
[24] Doubrawa P, Barthelmie R J, Wang H, Pryor S C and Churchfield M J 2016 *Remote Sens.* **11** 939